Academic Journal of Science and Technology
ISSN: 2771-3032 | Vol. 13, No. 1, 2024

A Preliminary Study on The Causes of the "Triple-peak" La Niña During 2020-2022

Yunnan Yang

Ocean University of China, Qingdao, Shandong, 266100, China

Abstract: The 2020-2022 triple-peak La Niña is the first consecutive three-year La Niña event in this century. In order to investigate the similarities and differences between this event and the other observed bimodal and triple events, this study uses synthetic and regression analysis, empirical orthogonal function decomposition, and mixed layer heat budget diagnosis to compare other events with this one in terms of location of anomalous negative sea surface temperature (SST), anomalous wind direction, and mixed layer heat budget. In the previous bimodal events, the centers of SST negative anomalies were both in the (5°S-5°N, 180°-120°W) region; there were anomalous northerly and westerly winds east of 140°W, and the negat precipitation anomalies were distributed along north of the equator. In contrast, the peak position of the second negative SST anomaly in this event is more eastward and southward; the anomalous easterlies continue from 120°E to the eastern boundary of the basin, and there is an anomalous southerlies in the eastern part of the basin. To further investigate the role of the anomalous easterlies and southerlies, this study calculates the mixed layer heat budget in key region. Corresponding to the latitudinal (longitudinal) wind anomalies, the latitudinal (longitudinal) temperature advection dominates the robust difference between the bimodal event and this triple-peak event. The anomalous easterlies and southerlies in the equatorial Pacific are favorable to the appearance of the third La Niña year in this event. This study is important in understanding the dynamics of triple-peak La Niña events, and will facilitate the forecast of such event.

Keywords: La Niña; Sea surface temperature; Anomalous southeasterlies; Ocean- atmosphere interaction.

1. Introduction

After an El Niño event, a La Niña event often occurs in the following year, and La Niña events can last for two to three consecutive years [1, 2, 3, 4].

Hu et al.[1] 2014 suggested that there are usually two conditions for consecutive La Niña events. The first condition is the presence of a strong La Niña event, which ensures that the reflected Rossby wave signal at the eastern boundary of the Pacific produces a strong westward-propagating cold sea temperature anomaly outside the equator. The cold anomaly outside the equator may hinder the recharge process along the equator, thus favoring the sustained presence of cold subsurface ocean temperature anomalies, and preventing the transition of La Niña to El Niño. The second condition is the presence of eastward-propagating downwelling Kelvin waves (Figure 1) during the decaying phase of a strong La Niña event. The activity of equatorial Kelvin waves is related to surface wind fluctuations in the far western equatorial Pacific, and the eastward-propagating downwelling Kelvin waves may lead to the demise of subsequent La Niña trends. In conclusion, the recharge/discharge processes in the equatorial Pacific and the surface winds in the far western equatorial Pacific are indicators of whether subsequent La Niña events will occur.

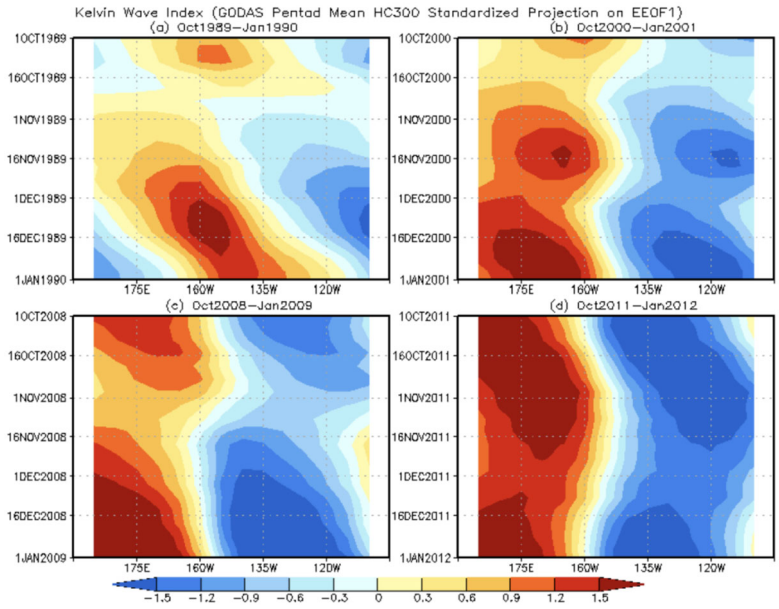

Figure 1. Standardized projection of pentad mean OTAs along the equator onto 1st mode of EEOF in (a) Oct 1989-Jan 1990, (b) Oct 2000- Jan 2001, (c) Oct 2008-Jan 2009, and (d) Oct 2011-Jan 2012. (Hu et al.[1])

According to Fang et al.[5], a four-variable linear regression model based on important ocean- atmosphere variables from the equatorial Pacific region in March 2022 were constructed to generate the corresponding time series plots. The results showed that, in 2022, the equatorial average ther- mocline depth anomaly (TCDa_M, Figure 2 (a)) and the zonal gradient of the equatorial Pacific thermocline average depth anomaly (TCDa_G, Figure 2 (b)) did not exhibit significant anomalies compared to previous years.

In contrast, atmospheric variables showed clear anomalies: the eastward wind stress (Tauxa_W, Figure 2 (c)) was comparable to that of 2000, while the southward wind stress (Tauya_E, Figure 2 (d)) reached its maximum amplitude in 1980. The study concluded that the southeasterly winds observed in the equatorial Pacific were favorable for the continuation of La Niña into the third year. The meridional processes in the eastern Pacific, which are often overlooked in classical ENSO theory, are crucial for accurately describing the evolution of ENSO after March [6, 7].

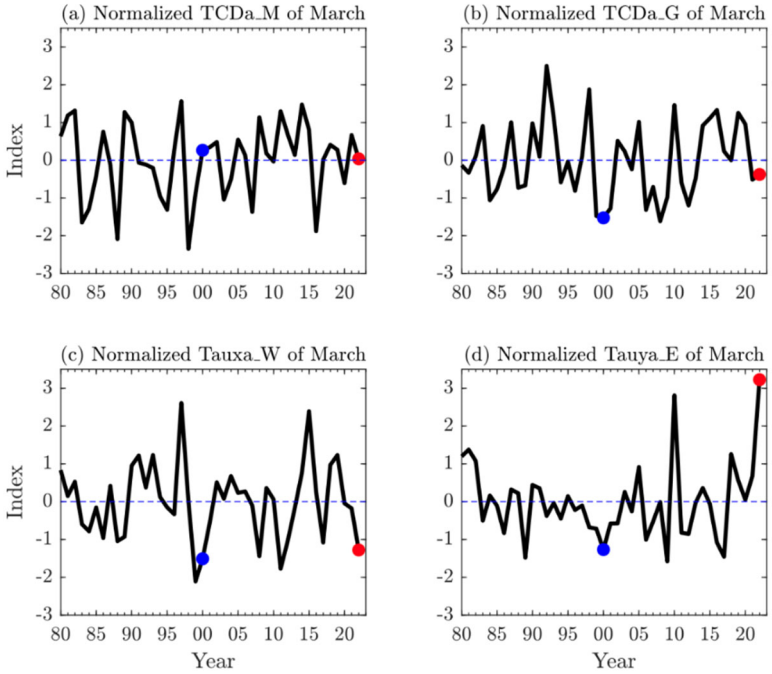

Figure 2. Normalized indices for (a)TCDa M, (b)TCDa G, (c)Tauxa W, and (d)Tauya E in March. In each panel, the blue and red dots represent 2000 and 2022, respectively. (Fang et al. [5])

From Figure 3, it can be seen that the strong easterly wind stress (Tauxa W) in 2000 overcame the opposing effects of the other three variables, indicating that the strong anomalous easterlies in the Western Pacific can induce upwelling Kelvin waves and drive anomalous westward surface currents, leading to cooling. In 2022, both the anomalous easterlies (Tauxa W) and southerlies (Tauya E) were important, each contributing approximately 50% of the growth rate. The southerly wind is thought to strengthen ocean upwelling south of the equator [7] and enhance the intrusion of subsurface cold water from off-equatorial regions into the equatorial region [2], thereby providing an additional cooling effect on SST variations.

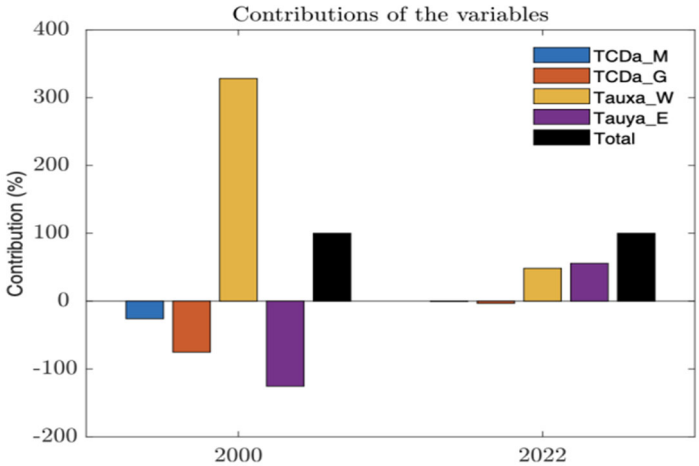

Figure 3. Contribution of each variable in March to the following OND mean Niño-3.4 index in 2000 (left) and 2022 (right). The blue, red, yellow, and purple bars represent the contribution percentages from TCDa M, TCDa G, Tauxa W, and Tauya E, respectively. The black bar is for the total (100%), i.e., the combination of the four components. (Fang et al. [5])

2. Data and Methods

2.1. Data Set

This article uses the data set in Table 1

Table 1. Ocean and atmosphere reanalysis data used in this paper

Variable	Resolution	Data Source	Website
Sea Surface Temperature	2° × 2° Monthly	ERSST v5	https://psl.noaa.gov/data/gridded/data.noaaglobaltemp.html
Precipitation	2.5° × 2.5° Monthly	CMAP	https://psl.noaa.gov/data/gridded/data.cmap.html
U (V) Wind	2.5° × 2.5° Monthly	NCEP reanalysis	https://psl.noaa.gov/data/gridded/data.ncep.reanalysis.html
U (V) of current	0.333° × 1° Monthlyy	GODAS	https://psl.noaa.gov/data/gridded/data.godas.html
Geometric vertical velocity	0.333° × 1° Monthly	GODAS	https://psl.noaa.gov/data/gridded/data.godas.htm
Potential Temperature	0.333° × 1° Monthly	GODAS	https://psl.noaa.gov/data/gridded/data.godas.html
Total downward heat flux at surface	0.333° × 1° Monthly	GODAS	https://psl.noaa.gov/data/gridded/data.godas.html

2.2. Methods

2.2.1. Data Preprocessing Method

Because different variables have different spatial resolutions, this article first interpolates all mete- orological variables onto a uniform 2°×2° space grid. This makes it easier to process and analyze them together. The steps for extracting anomaly signals are as follows:

1. Detrend each point on the latitude and longitude grid.
2. Calculate the anomaly from month to month, to remove the seasonal cycle signal of the climatological state.

2.2.2. Definition of Bimodal Events

To study the unique features of this event, we selected all La Niña events since 1980 that lasted two consecutive years (1983-1984, 2007-2008, 2010-2011, 2016-2017). We also included the year following each event. These events were combined to form the bimodal events.

2.2.3. Definition of Year Representation

Jan(0) represents January of the year before the first SST negative anomaly peak in the La Niña event. Jan(1) is January of the year after the first peak, and Jan(2) is January of the year after the second peak, and so on.

2.2.4. Index Definition

The Niño 3 and Niño 4 indices, related to ENSO, are defined as the interannual anomaly signals in the regions (5°S-5°N, 150°W-90°W) and (5°S-5°N, 160°E-150°W), respectively.

2.2.5. Statistical Methods

We used common meteorological statistical methods in this paper, including the regression coefficient test (t-test), Empirical Orthogonal Function (EOF) decomposition, and power spectrum analysis.

2.2.6. Diagnostic methods of the oceanic mixed-layer heat budget

$$\frac{\partial T'}{\partial t} = \begin{array}{l} \frac{Q'_{net}}{\rho_0 c_p H_m} - \left(u'\frac{\partial \overline{T}}{\partial x} + \overline{u}\frac{\partial T'}{\partial x} + u'\frac{\partial T'}{\partial x}\right) \\ -\left(v'\frac{\partial \overline{T}}{\partial y} + \overline{v}\frac{\partial T'}{\partial y} + v'\frac{\partial T'}{\partial y}\right) \\ -\left(w'_b\frac{\overline{T}-\overline{T_b}}{H_m} + \overline{w_b}\frac{T'-T'_b}{H_m} + w'_b\frac{T'-T_b}{H_m}\right) + R \end{array} \quad (1)$$

In equation 1, Qnet is the net heat flux at thesea surface (Positive downwards means that the ocean gets hot). It includes shortwave radiation, longwave radiation, and sensible and latent heat fluxes. ρ_0 is the density of seawater (1025 kg/m^3, treated as a constant), and C_p is the specific heat of seawater (3850 J kg^{-1}K^{-1}). Hm is the depth of the mixed layer, which is set to the depth of the 6th layer of GODAS data, i.e., 55 m. The average of the first five layers of GODAS data (0-45 m) is used for calculations involving the vertically averaged variables of the mixed layer. u and v are the zonal and meridional flow velocities, respectively, averaged vertically within the mixed layer. T is the vertically averaged oceanic temperature of the mixed layer. wb and Tb are the vertical velocity and temperature at the bottom of the mixed layer. The symbol ($'$) indicates interannual anomalies, while the overbar represents the climatological mean state. R is a residual term that includes other processes not considered by the main terms, such as shortwave radiation penetrating below the mixed layer, vertical entrainment, and subgrid-scale processes.

Equation 1 breaks down the mixed layer temperature anomaly into 11 terms on the right-hand side. The first term represents the heating rate due to air-sea heat exchange, indicating the thermal feedback between the ocean and the atmosphere. The 2nd, 3rd, and 4th terms are zonal temperature advection, where u' represents anomalous zonal current, and $\frac{\partial T'}{\partial x}$ is the anomalous zonal temperature gradient. The 5th, 6th, and 7th terms are meridional temperature advection, where v' represents anomalous meridional current, and $\frac{\partial T'}{\partial y}$ is the anomalous meridional temperature gradient. The 8th, 9th, and 10th terms represent temperature advection across the bottom of the mixed layer. The 8th term indicates Ekman feedback, while the 9th represents thermocline feedback.

3. Comparison of Meteorological Element Fields

3.1. Meridional Mean

During the double-peak events, anomalous northerly winds accompanied the appearance of the two cold centers in the equatorial eastern Pacific region, whereas in the current triple-peak event, per- sistent southerly winds prevailed throughout its lifespan. Since the climatological state SST in the southern part of the eastern Pacific is lower than in the northern part, the southerly winds during this event transported cold signals from outside the equator into the equatorial region through cold ad-vection, resulting in temperature gradient changes between the Northern and Southern Hemispheres, and triggering the Wind-Evaporation-SST (WES) mechanism, which further maintained the SST differences between the two hemispheres.

During the double-peak events, easterlies prevailed west of

140°W, while westerlies prevailed east of 140°W, (Figure 4). However, during the current event, easterlies prevailed from 120°E to the coast of South America. According to the Bjerknes positive feedback mechanism, the strengthening of easterlies along the equator will be through the coupling between SST-winds-thermocline, thereby strengthening the gradient of anomalous SST between the east and west, and further expanding the area of easterly anomalies. The anomalous easterlies could affect the large-scale Walker circulation, leading to a consecutive three-year La Niña event. The southerly and easterly wind components in the current event continuously introduce cold SST signals into the equatorial eastern Pacific, which is one of the main reasons for the consecutive three-year La Niña event from 2020 to 2022.

Additionally, during the double-peak events, the two cold centers appeared during Oct(0)-Jan(1) and Oct(1)-Jan(2), located in the central Pacific region between 180° and 120°W. In contrast, during the current triple-peak event, the cold center during the Oct(1)-Jan(2) stage was significantly farther east, appearing in the 120°W-90°W region, which is related to the prevailing anomalous easterlies and southerlies.

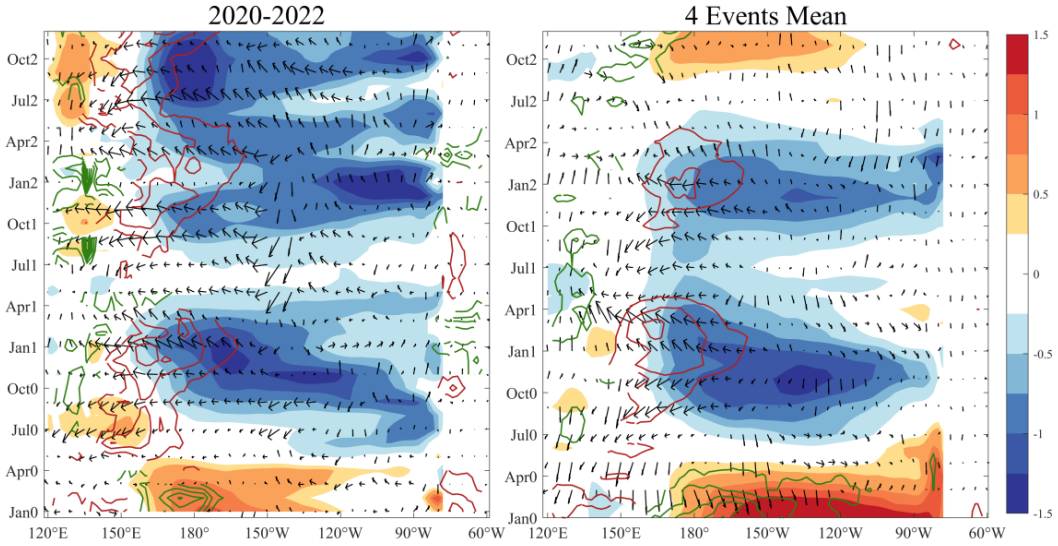

Figure 4. Meridional mean of the 2020-2022 triple-peak La Niña event and the bimodal event at (5°S-5°N, 120°E-60°W). SST anomaly (shading; unit: °C); precipitation anomaly (contour interval 2mm, red/green contours denote negative/positive precipitation anomalies), and 1000hPa anomaly winds (vector; unit: m/s)

Compared to the triple-peak La Niña event that developed from a strong El Niño event in 1998- 2000, the current event originated from a weaker central-type El Niño, but the range and intensity of negative SST anomalies in the eastern Pacific were not inferior to those of the 1998 event. The cold center positions during the Jul(0)-Jan(1) (Figure 5) period were relatively consistent for both triple-peak events, whereas during the Oct(1)-Jan(2) period, the cold center in the current event shifted significantly eastward, which may be related to the anomalous southeasterlies. In addition, both events showed an anomalous cold center in the western Pacific during Oct(2)-Jan(3).

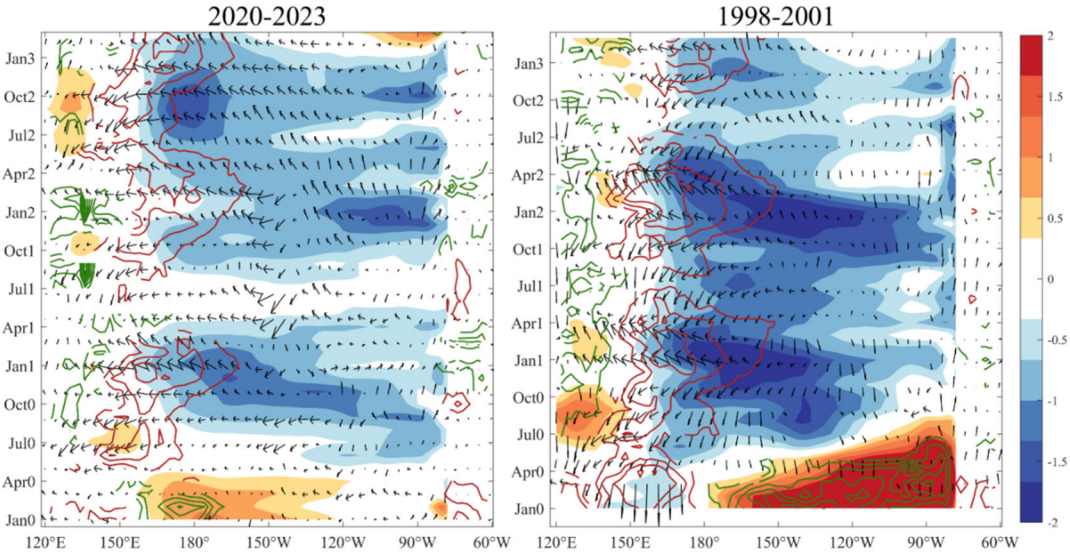

Figure 5. Meridional mean of the triple-peak La Niña events in 2020-2023 and 1998-2001 at (5°S-5°N, 120°E-60°W). SST anomaly (shading; unit: °C); precipitation anomaly (contour interval 2mm, red/green contours denote negative/positive precipitation anomalies), and 1000hPa anomaly winds(vector; unit: m/s)

3.2. Temporal Evolution Characteristics of Wind Fields

To visually compare the differences in the anomalous wind fields between the current event, the double-peak events, and the 1998-2000 triple-peak event, time series plots of the anomalous wind fields in the Niño 4 and Niño 3 regions were created.

In the Niño 4 region (Figure 6), all three events exhibit strong anomalous westerlies (U-wind) from Jan(0) to Apr(0). During the Apr(2)-Oct(2) period, the current event shows significantly stronger anomalous easterlies compared to the double-peak and 1998 events. The 1998 event exhibits clear northerly anomalies (V-wind) from Jan (0) to Oct(0), while there are no significant meridional wind anomalies from Jan(1) to Jan(2) for all three events. However, the current event displays a clear southerly anomaly from Apr(2) to Oct(2).

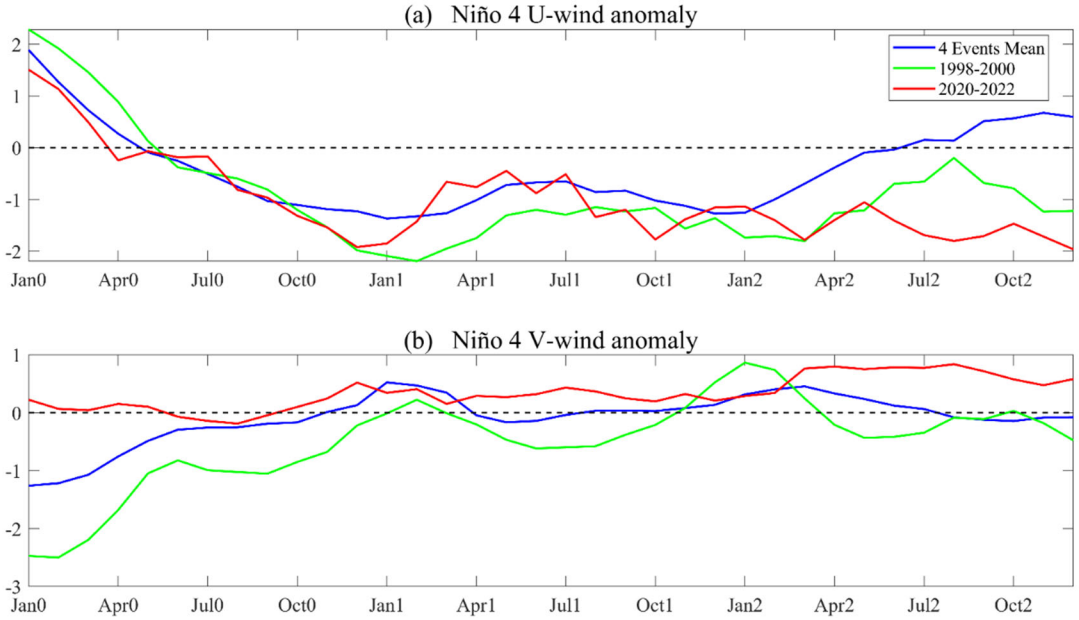

Figure 6. Temporal evolution of the anomalous winds (unit: m/s) in the Niño 4 region during the bimodal event (blue line), the 1998-2000 event (green line) and the 2020-2022 event (red line)

In the Niño 3 region (Figure 7), the 1998 event shows strong anomalous westerlies from Jan(0) to Jul(0). The double-peak event has relatively small meridional wind anomalies, with prevailing anomalous westerlies most of the time. In contrast, the current event has almost no westerly anomalies throughout its lifespan, with anomalous easterlies being much stronger than in the other two events. The 1998 event exhibits clear northerly anomalies from Jan(0) to Jan(1). From Apr(1) to Jan(2), none of the three events show significant meridional wind anomalies, but the current event displays a clear southerly anomaly from Oct(1) to Oct(2).

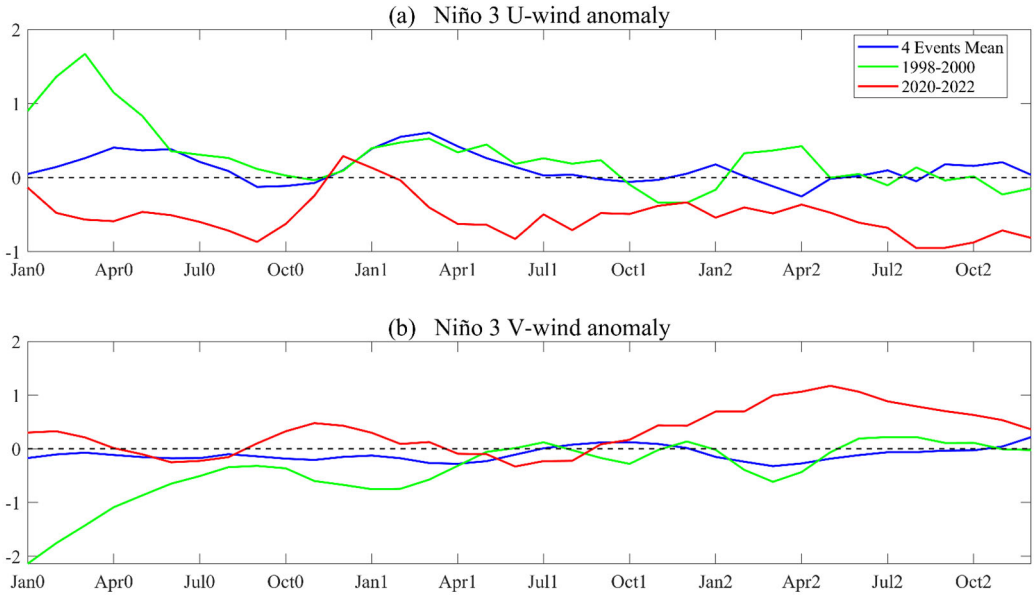

Figure 7. Temporal evolution of the anomalous winds (unit: m/s) in the Niño 3 region during the bimodal event (blue line), the 1998-2000 event (green line) and the 2020-2022 event (red line)

3.3. Spatial Evolution Characteristics of SST and Wind Field Distributions

East of 150°W, the double-peak events feature prevailing northerlies, while the current event is characterized by prevailing southerlies. The SST negative anomaly field during March-May 2022 (Figure 8(d)) aligns with the trend of the anomalous southeasterly winds, indicating that the anoma- lous easterly and southerly components of the current event may have contributed significantly to the persistence of the La Niña event into the third year.

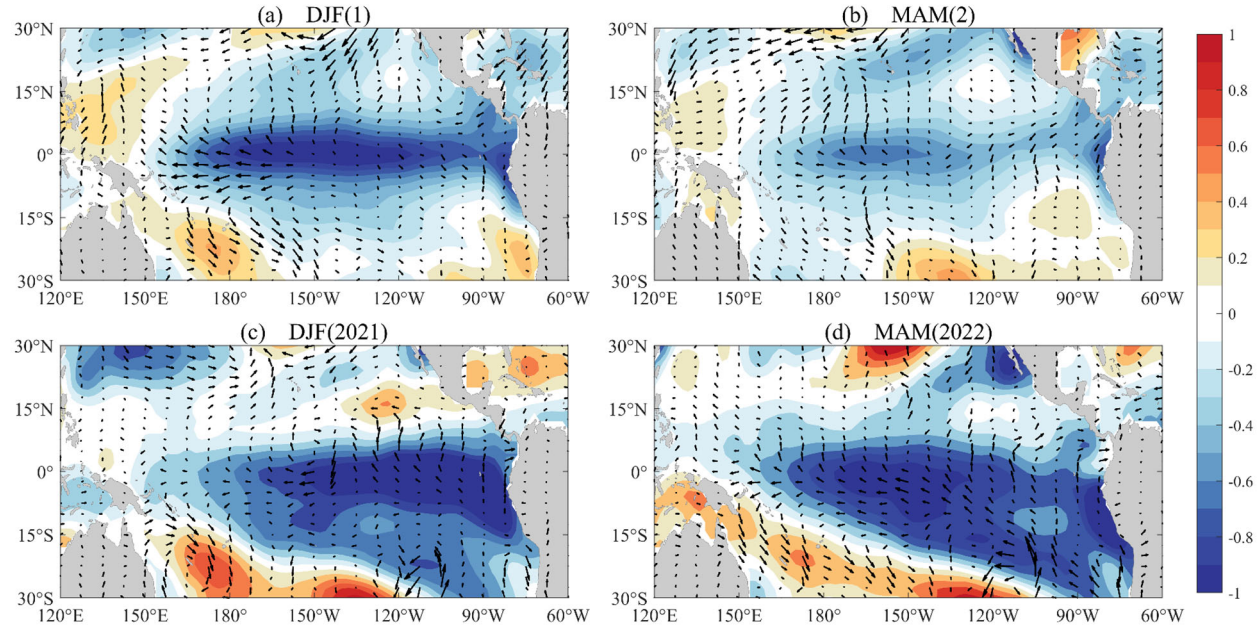

Figure 8. Spatial distribution of the bimodal event and the 2020-2022 triple-peak event averaged every three months from Jun(0)-Nov(2) (partial). SST anomaly (shading; unit: °C) and anomalous winds (vector; unit: m/s)

In the 1998 event, the SST cold anomaly was positioned farther north, which was particularly evident during MAM(2000) and MAM(2022) (Figure 9). Similar to the double-peak events, the 1998 event exhibited strong anomalous easterlies in the western Pacific. East of 120°W, the 1998 event featured anomalous northwesterly winds, while the current event had anomalous southeasterly winds. The wind direction influenced the position of the SST cold anomaly, causing the SST negative anomaly in the current event to be positioned further south and east.

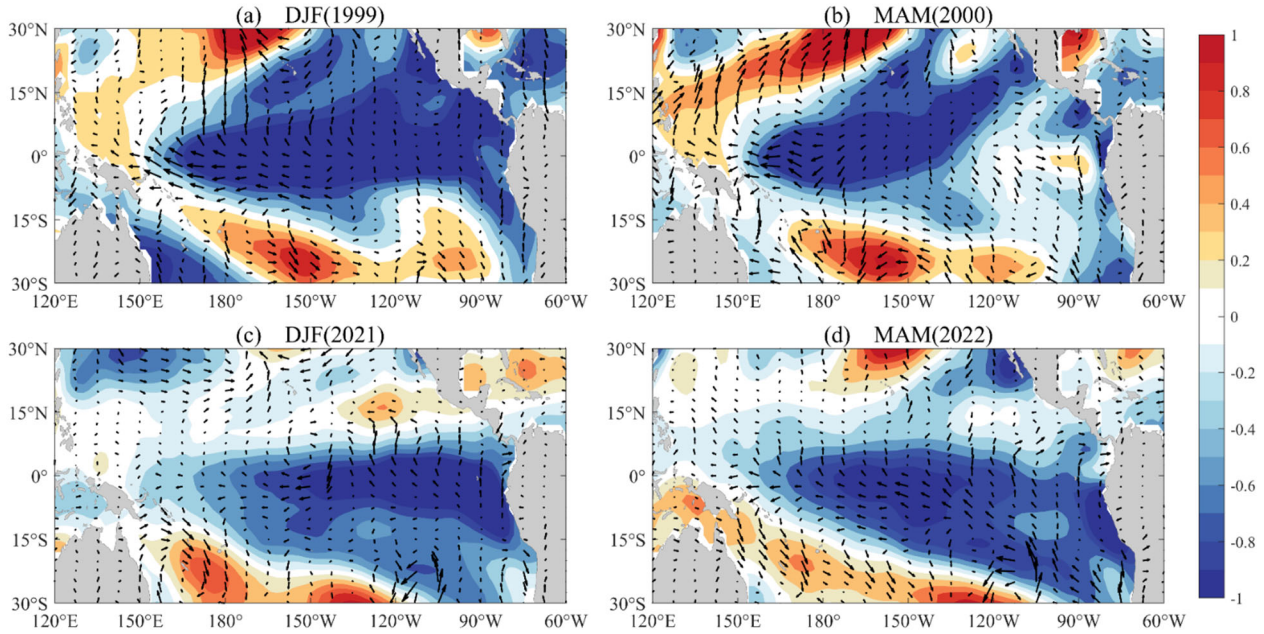

Figure 9. Spatial distribution of the bimodal event and the 2020-2022 triple-peak event averaged every three months from Jun(0)-Nov(2) (partial). SST anomaly (shading; unit: °C) and anomalous winds (vector; unit: m/s)

4. Precipitation EOF Analysis

EOF analysis was performed on the precipitation anomaly field from February to April (FMA) for the years 1979-2022. The leading principal component (PC1) and the second principal component (PC2) were regressed against the anomalous wind field and SST anomaly field, and the results were presented as wind arrows and contour lines (Figure 10 a, c). Time series for the first and second principal components were also plotted (Figure 10 b, d) and compared with the time series of the Niño 3 and Niño 4 indices, with correlation coefficients calculated.

The leading principal component of FMA precipitation changes accounts for 47% of the total vari- ance, characterized by an increase in precipitation centered around the equator. The first mode of EOF (EOF1) captures the so-called "extreme El Niño" events, which correspond to strong convection [8, 9] and heavy precipitation in the eastern Pacific Niño 3 region [10, 11]. Analysis of the time series shows that PC1 is correlated with the Niño 3 index (correlation coefficient r = 0.74). PC1 is dominated by the strong El Niño events of 1983 and 1998 and also includes two weaker events from 1987 and 1992 (Figure 10a). Extreme ENSO events can trigger the Bjerknes positive feedback mechanism, counteracting the decline of El Niño: a sufficiently strong El Niño raises the equatorial SST above the convection threshold [12], triggering anomalous equatorial precipitation. The anoma- lous precipitation will cause westerly wind anomalies to invade the eastern equatorial Pacific, thereby weakening the equatorial upwelling in the eastern Pacific and maintaining the warming trend of SST in that region. The westerly wind anomaly invasion and SST warming in the eastern Pacific form positive feedback, offsetting the rapid attenuation of equatorial wind anomalies in the central Pacific after December, thus slowing the decline of extreme El Niño events.

The second mode of EOF accounts for 20% of the total variance, with the precipitation anomaly field exhibiting a north-south antisymmetric mode, where the bands of increased (decreased) rainfall are concentrated around 5°N (6°S), roughly aligning with the climatological rainfall belt of FMA. Moderate-intensity ENSO events trigger the Eastern Pacific ITCZ Dipole (EPID) mode through the WES mechanism [7]: anomalous southeasterly winds strengthen the southeasterly trades south of the equator, enhancing surface evaporation and lowering SST. North of the equator, the anomalous southeasterlies weaken the trades, reduce evaporative cooling, and increase SST, thereby generating the EPID mode. The southeasterlies crossing the equator in March (Figure 10c) enhance upwelling south of the equator, rapidly cooling that region. The resulting cold advection weakens the SST north of the equator, leading to the rapid dissipation of moderate El Niño events. PC2 is correlated with the central Pacific Niño 4 index (correlation coefficient r = 0.62). Typically, during La Niña events, the precipitation anomaly field shows a pattern of less rainfall in the north and more in the south; however, in this event, PC2 < 0 indicates a pattern of more rainfall in the north and less in the south, corresponding to the southerlies crossing the equator, which favor upwelling south of the equator and northward cold oceanic advection, slowing the SST decay rate. This could be one of the reasons why this event lasted for three years.

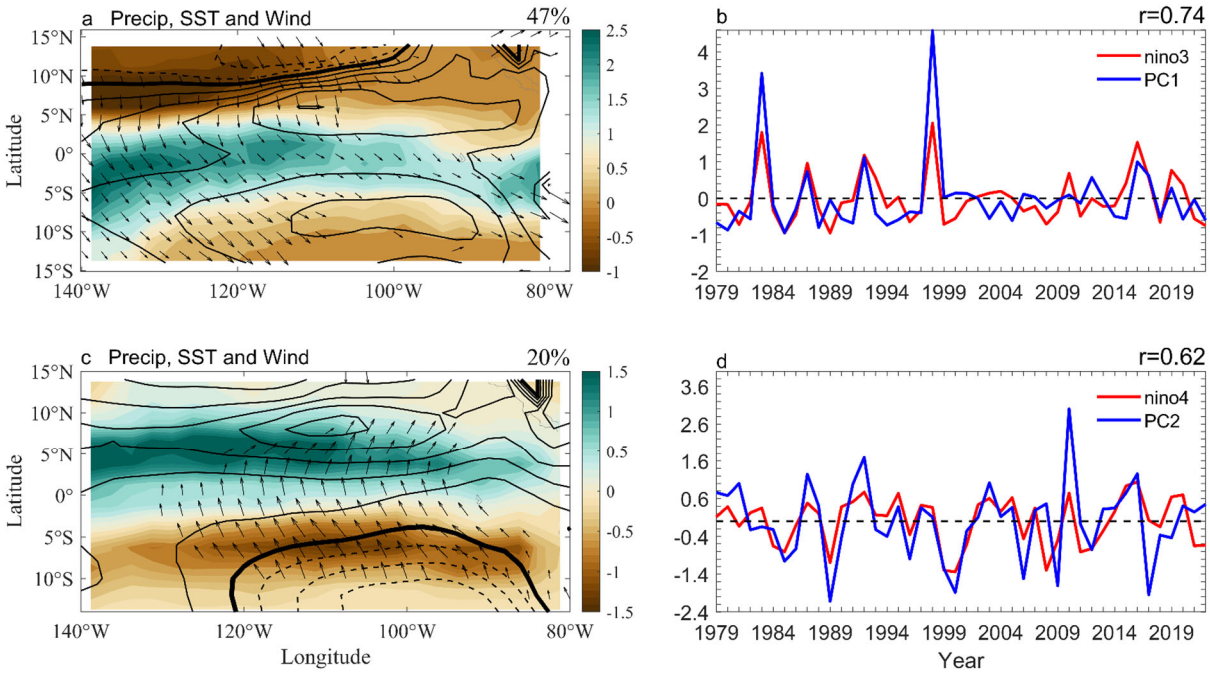

Figure 10. EOF model of rainfall variability in the eastern tropical Pacific FMA. Regressions of a, c rainfall(colored shading), SST (contour interval 0.3°C, 0 bolded, negative as dashed line) and surface wind (m/s; vector arrows) relative to b, d standardized PC (blue); correlation (r) is significant at 95% confidence level based on t-test. Plotted in red are the b eastern (Niño 3) and (d) central (Niño 4) equatorial Pacific SST indices that occurred during the same period.

5. Ocean Mixed-Layer Heat Budget Diagnosis

5.1. Niño 4 Region

In the Niño 4 region, this event shows a clear positive mixed-layer temperature anomaly tendency trend in Apr(1) and a clear negative trend in Oct(1), while the bimodal event does not have a clear positive or negative trend (Figure 11 (a), (b)).

The change in zonal temperature advection is mainly contributed by the $-u'\frac{\partial \overline{T}}{\partial x}$ term (Figure 11 (c), (d)). When $-u'\frac{\partial \overline{T}}{\partial x} < 0$, it means that the anomalous westward current reduces the positive SST in this region under the west-warm and east-cool SST climatological pattern. From Apr(0) to Oct(0), both events have negative zonal temperature advection with similar strengths. In Apr(1) and Oct(1), both events show positive and negative zonal temperature advection anomalies, respectively, but this event has a stronger effect than the bimodal event. After Apr(2), this event continues to have negative zonal advection anomalies, while the bimodal event turns positive. This shows that the bimodal event shifts from an abnormal westward current to an abnormal eastward current, marking the end of the La Niña event.

The difference in meridional temperature advection between the two events is mainly from $-v'\frac{\partial \overline{T}}{\partial y}$ term (Figure 11 (e), (f)). After Apr(0), both events shift from positive to negative meridional tem- perature advection, and both have negative anomalies from Jul(0) to Jan(2). From Apr(2) to Oct(2), this event still has strong negative meridional advection, while the bimodal event turns positive.

The change in temperature advection across the mixed-layer base mainly comes from the $-\overline{W_b}\frac{T'-T_b'}{H_m}$ term (Figure 11 (g), (h)). From Jan(0) to Oct(1), neither event has significant temperature advection across the mixed-layer base. This event has negative and positive advection anomalies in Jan(2) and Jul(2), respectively, while the bimodal event shows a gradually increasing negative anomaly after Jan(2).

5.2. Niño 3 Region

In the Niño 3 region, both the bimodal event and this event show a weak negative trend from Jul(0) to Oct(0) (Figure 12 (a), (b)). This event has a strong negative trend in Oct(1) and Oct(2), while the bimodal event shows a clear positive trend in Apr(1) and Apr(2). Both zonal and meridional temperature advection make significant contributions.

In Oct(0), the strength of the negative zonal temperature advection anomalies is similar in both events (Figure 12 (c), (d)). In Oct(1), this event shows a much stronger negative anomaly than the bimodal event, indicating a strong westward current that reduces SST. In Oct(2), this event still shows a negative anomaly, while the bimodal event turns positive, showing that the bimodal event's current shifts from westward to eastward.

The first strong negative anomaly in meridional temperature advection appears in Oct(0) for this event and in Jul(0) for the bimodal event (Figure 12 (e), (f)). The second negative anomaly occurs in Oct(1), where the bimodal event's negative anomaly weakens significantly. In Oct(2), this event continues to show a negative anomaly, while the bimodal event shows a positive anomaly.

From Jan(0) to Jan(1), both events have negative temperature advection anomalies across the mixed-layer base (Figure 12 (g), (h)). In Oct(1) and Oct(2), this event's strength is greater than the bimodal event's. In Apr(1) and Apr(2), both events show weak positive anomalies.

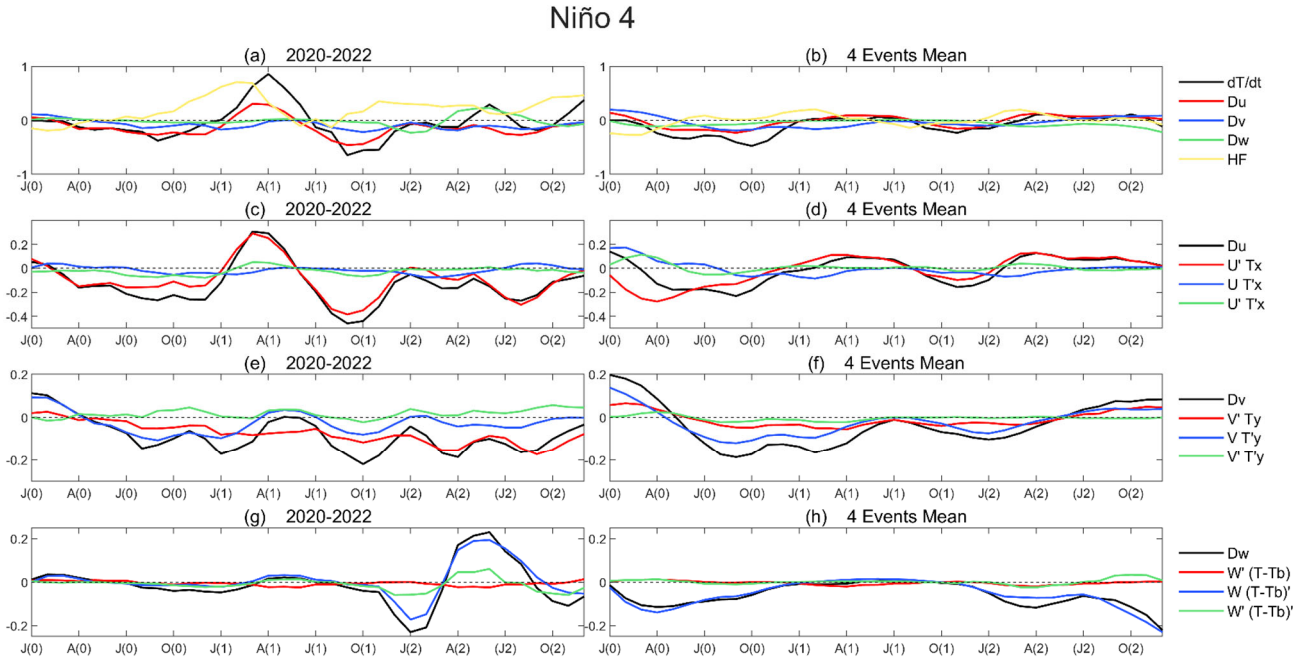

Figure 11. Ocean mixed layer heat balance for La Niña and bimodal events in Niño 4 area for 2020-2022(unit: °C/month)

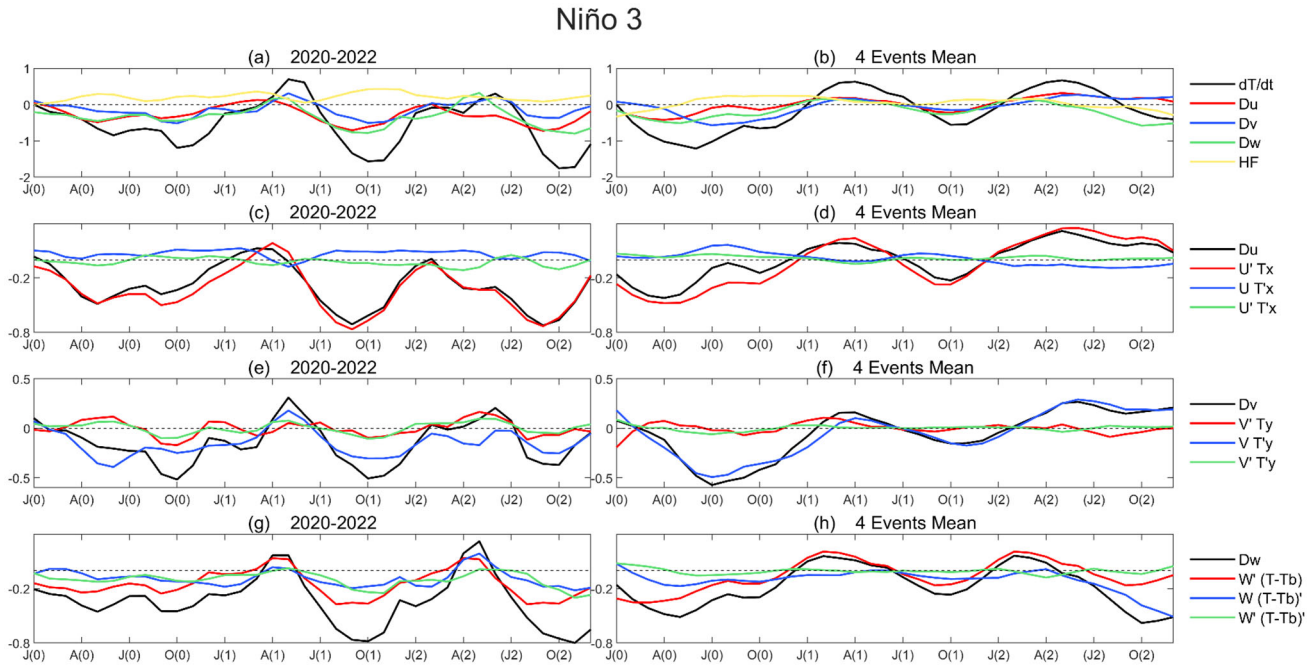

Figure 12. Ocean mixed layer heat balance for La Niña and bimodal events in Niño 3 area for 2020-2022(unit: °C/month)

References

[1] Zeng-Zhen Hu, Arun Kumar, Yan Xue, and Bhaskar Jha. Why were some La Niñas followed by another La Niña? Climate Dynamics, 42:1029–1042, 2014.

[2] Fei Zheng, Lisha Feng, and Jiang Zhu. An incursion of off-equatorial subsurface cold water and its role in triggering the "double dip" La Niña event of 2011. Advances in Atmospheric Sciences, 32:731–742, 2015.

[3] Pedro N DiNezio, Clara Deser, Alicia Karspeck, Stephen Yeager, Yuko Okumura, Gokhan Dan- abasoglu, Nan Rosenbloom, Julie Caron, and Gerald A Meehl. A 2 year forecast for a 60–80% chance of La Niña in 2017–2018. Geophysical Research Letters, 44(22):11–624, 2017.

[4] Xian Wu, Yuko M Okumura, Clara Deser, and Pedro N DiNezio. Two-year dynamical predictions of enso event duration during 1954–2015. Journal of Climate, 34(10):4069–4087, 2021.

[5] Xianghui Fang, Fei Zheng, Kexin Li, Zeng-Zhen Hu, Hongli Ren, Jie Wu, Xingrong Chen, Weiren Lan, Yuan Yuan, Licheng Feng, et al. Will the historic southeasterly wind over the equatorial pacific in march 2022 trigger a third-year La Niña event?, 2023.

[6] Shineng Hu and Alexey V Fedorov. Cross-equatorial winds control El Niño diversity and change. Nature Climate Change, 8(9):798–802, 2018.

[7] Shang-Ping Xie, Qihua Peng, Youichi Kamae, Xiao-Tong Zheng, Hiroki Tokinaga, and Dongxiao Wang. Eastern pacific itcz dipole and enso diversity. Journal of Climate, 31(11): 4449–4462, 2018.

[8] Andrew M Chiodi and Don E Harrison. El Niño impacts on seasonal us atmospheric circulation, temperature, and precipitation anomalies: The olr-event perspective. Journal of Climate, 26 (3):822–837, 2013.

[9] Nathaniel C Johnson and Yu Kosaka. The impact of eastern equatorial pacific convection on the diversity of boreal winter El Niñoteleconnection patterns. Climate Dynamics, 47 (12): 3737–3765, 2016.

[10] Wenju Cai, Simon Borlace, Matthieu Lengaigne, Peter Van Rensch, Mat Collins, Gabriel Vecchi, Axel Timmermann, Agus Santoso, Michael J McPhaden, Lixin Wu, et al. Increasing frequency of extreme El Niño events due to greenhouse warming. Nature climate change, 4(2):111–116, 2014.

[11] Ken Takahashi, Aldo Montecinos, Katerina Goubanova, and Boris Dewitte. Enso regimes: Reinterpreting the canonical and modoki El Niño. Geophysical research letters, 38(10), 2011.

[12] Nathaniel C Johnson and Shang-Ping Xie. Changes in the sea surface temperature threshold for tropical convection. Nature Geoscience, 3(12):842–845, 2010.